Electrodeposition of Zn and Cu−Zn alloy from ZnO/CuO precursors in deep eutectic solvent

Xie, Xueliang; Zou, Xingli; Lu, Xionggang; Lu, Changyuan; Cheng, Hongwei; Xu, Qian; Zhou, Zhongfu

Published in:
Applied Surface Science

DOI:
10.1016/j.apsusc.2016.05.138

Publication date:
2016

Citation for published version (APA):
Xie, X., Zou, X., Lu, X., Lu, C., Cheng, H., Xu, Q., & Zhou, Z. (2016). Electrodeposition of Zn and Cu−Zn alloy from ZnO/CuO precursors in deep eutectic solvent. *Applied Surface Science*, *385*, 481-489. https://doi.org/10.1016/j.apsusc.2016.05.138

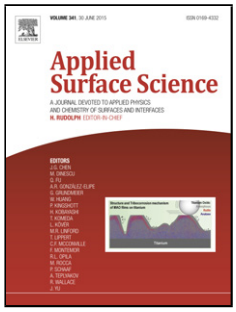

Title: Electrodeposition of Zn and Cu−Zn alloy from ZnO/CuO precursors in deep eutectic solvent

Author: Xueliang Xie Xingli Zou Xionggang Lu Changyuan Lu Hongwei Cheng Qian Xu Zhongfu Zhou

PII: S0169-4332(16)31168-0
DOI: http://dx.doi.org/doi:10.1016/j.apsusc.2016.05.138
Reference: APSUSC 33331

To appear in: *APSUSC*

Received date: 27-1-2016
Revised date: 24-5-2016
Accepted date: 25-5-2016

Please cite this article as: Xueliang Xie, Xingli Zou, Xionggang Lu, Changyuan Lu, Hongwei Cheng, Qian Xu, Zhongfu Zhou, Electrodeposition of Zn and Cu−Zn alloy from ZnO/CuO precursors in deep eutectic solvent, Applied Surface Science http://dx.doi.org/10.1016/j.apsusc.2016.05.138

Electrodeposition of Zn and Cu−Zn alloy from ZnO/CuO precursors in deep eutectic solvent

Xueliang Xie[a], Xingli Zou[a,*], Xionggang Lu[a,*], Changyuan Lu[a], Hongwei Cheng[a], Qian Xu[a], Zhongfu Zhou[a,b]

[a] *State Key Laboratory of Advanced Special Steel & Shanghai Key Laboratory of Advanced Ferrometallurgy & School of Materials Science and Engineering, Shanghai University, Shanghai 200072, P. R. China.*

[b] *Institute of Mathematics and Physics, Aberystwyth University, Aberystwyth SY23 3BZ, UK.*

* Corresponding authors: Tel. & fax: +86-21-56335768. E-mail addresses: *xinglizou@shu.edu.cn* (X. Zou); *luxg@shu.edu.cn* (X. Lu)

Graphical abstract

Micro/nanostructured Zn and Cu−Zn alloy films have been electrodeposited directly from ZnO/CuO precursors in ChCl/urea-based DES, the typical nucleation-growth mechanism and the micro/nanostructures-formation process are determined.

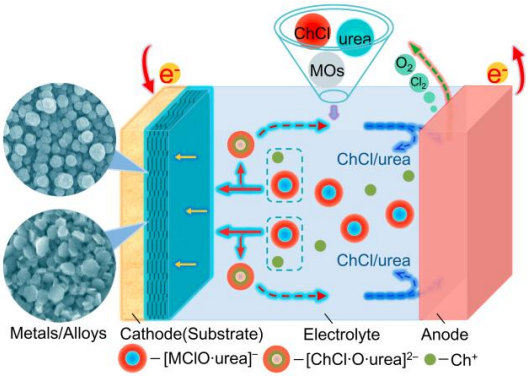

Highlights

> Micro/nanostructured Zn films have been electrodeposited directly from ZnO precursor in deep eutectic solvent (DES).

> The morphology of the Zn electrodeposits depends on the cathodic potential and temperature.

> The electrodeposited Zn films exhibit homogeneous morphologies with controllable particle sizes and improved corrosion resistance.

> Cu–Zn alloy films have also been electrodeposited directly from their metal oxides precursors in DES.

Abstract The electrodeposition of Zn and Cu−Zn alloy has been investigated in choline chloride (ChCl)/urea (1:2 molar ratio) based deep eutectic solvent (DES). Cyclic voltammetry study demonstrates that the reduction of Zn(II) to Zn is a diffusion-controlled quasi-reversible, one-step, two electrons transfer process. Chronoamperometric investigation indicates that the electrodeposition of Zn on a Cu electrode typically involves three-dimensional instantaneous nucleation with diffusion-controlled growth process. Micro/nanostructured Zn films can be obtained by controlling the electrodeposition potential and temperature. The electrodeposited Zn crystals preferentially orient parallel to the (101) plane. The Zn films electrodeposited under more positive potentials and low temperatures exhibit improved corrosion resistance in 3 wt% NaCl solution. In addition, Cu–Zn alloy films have also been electrodeposited directly from CuO–ZnO precursors in ChCl/urea-based DES. The XRD analysis indicates that the phase composition of the electrodeposited Cu–Zn alloy depends on the electrodeposition potential.

Keywords: Electrodeposition; Nucleation-growth kinetics; Deep eutectic solvent; Metal oxides; Morphology

1. Introduction

The electrodeposition of Zn and its alloys for the corrosion-resistant coatings and electrochemical applications such as electronics and batteries has received considerable attention in recent years [1–3]. Traditional Zn plating is performed mainly in sulfuric acidic aqueous baths where hydrometallurgical processes can occur [4,5]. Generally, Zn is extracted from zinc sulfide mineral ore. The ore is mined and beneficiated by flotation methods that produce zinc sulfide mineral concentrates. The wet concentrates are oxidized to metal oxides during high temperature roasting in air and then the metal oxides are leached with aqueous sulfuric acid. Finally, the Zn electrodeposits are produced from a zinc sulfate solution under current control [6,7]. However, the traditional Zn production is very sensitive to impurities and requires rigorous purification methods to obtain pure Zn [8]. Consequently, searching for new alternative eco-friendly electrolyte for electrodeposition of Zn and its alloys films at low temperature is needed.

More recently, the direct electrochemical reduction of metal oxides/compounds to metals/alloys in molten salts has been extensively investigated due to its environmental compatibility and low energy consumption [9,10]. These previous innovative work suggest that the production of metallic/coating materials direct from their metal oxides precursors in liquid salt is a promising route. Low-temperature electrolytic production of iron film from iron oxide in alkaline solution has been investigated in our recent work [11], which shows an acceptable current efficiency and the electrochemical process can be controlled effectively. However, in comparison with aqueous solutions, room temperature ionic liquids (RTILs) have been

gradually considered as promising electrolyte candidates to instead of the traditional aqueous electrolytes for metals/alloys electrodeposition [12]. RTILs have remarkable characteristics such as high thermal and chemical stability, negligible vapor pressure, high ionic conductivity, wide electrochemical windows and good solubility for quite a lot of metal salts [13,14]. The hydrogen evolution reactions and hydrogen embrittlement occurred in aqueous solutions can be therefore avoided by using ionic liquids as electrolytes. Electrodeposition of Zn in ionic liquids, especially in $AlCl_3$-based ionic liquids [15] and chlorozincate ionic liquids systems [16] has been investigated intensively. Recently, electrodeposition of Zn from $ZnCl_2$ has also been investigated in choline chloride (ChCl) based deep eutectic solvents (DESs) [17–21]. The nature of the DESs plays a significant role in the electrochemical behavior of Zn^{2+} ions, and the structure of the double layer seems to affect the Zn nucleation and thus can influence the morphology of the Zn electrodeposits in DESs [19]. Abbott et al. [19] investigated the electrodeposition of Zn in ionic liquids based on ChCl with either urea or ethylene glycol (EG). The significant differences were found in the chronoamperometric and gravimetric data, as well as in the morphology of the Zn deposit for both DESs. The different electrodeposition rates are probably attributed to the different chloride activities in the DESs, which changing the zinc concentration in the double layer and the electrodeposition mechanism of zinc. In addition, the influences of additives on the electrodeposition of Zn in DESs have also been investigated in the previous work [20,21]. Furthermore, Simons et al. [22] studied the dissolution and electrodeposition of Zn^{2+} in 1-ethyl-3-methylimidazolium dicyanamide ([EMIm]DCA). Liu et al. [23] illustrated the electrodeposition Zn films from zinc triflate ($Zn(TfO)_2$) in 1-butyl-1-methylpyrrolidinium trifluoromethylsulfonate ($[Py_{1,4}]TfO$) and

1-ethyl-3-methylimidazolium trifluoromethylsulfonate ([EMIm]TfO) ionic liquids. Zheng et al. [24] reported the electrodeposition of Zn coatings from ZnO in imidazolium chloride/urea ionic liquid, which showed that ZnO has considerable solubility in the ionic liquid.

DESs comprising ChCl with either urea or EG, have been successfully used as powerful and potential electrolytes for extracting metals from their corresponding metal oxides precursors, due to their highlighted advantages, such as biodegradable, relatively low cost, simple to prepare and relatively stable in air and moisture [25–31]. Moreover, the capability of DESs to selectively dissolve metal oxides is beneficial to the electrodeposition process. Only ZnO, Cu_2O and PbO_2 exhibit appreciable solubilities (ZnO: 0.123 M; Cu_2O: 0.072 M; PbO_2: 0.045 M) in ChCl/urea-based DES at 333 K, whereas other metal oxides such as CaO, SiO_2 and Al_2O_3 have negligible solubilities in the solvent [32,33]. In comparison with $ZnCl_2$ precursor [17–21], ZnO has potential to be used directly as a new promising precursor for the electrodeposition of Zn film in DES without chloridization pretreatment. ChCl/urea-based DES has been investigated as a potential solvent for Zn recovery from waste oxide residues [34], and Zn can be electrodeposited directly from ZnO precursor in ChCl/urea-based ionic liquid [25,26]. However, the detailed nucleation-growth kinetics of Zn electrodeposition process in ChCl/urea-based DES and the influences of experimental parameter on the final morphology of Zn electrodeposits still need more investigation.

In the present study, cyclic voltammetry (CV) and chronoamperometric measurements have been used to investigate the electrochemical reaction mechanism and the nucleation-growth process of Zn in ChCl/urea-based DES. The influences of electrodeposition potential and temperature on the morphology of Zn electrodeposits were examined. The

microstructure and the corrosion resistance of the obtained Zn films were investigated. In addition, Cu–Zn alloy films have also been electrodeposited from CuO–ZnO precursors in ChCl/urea-based DES.

2. Experimental

2.1. Electrolyte preparation

ChCl [$HOC_2H_4N(CH_3)_3Cl$] (Aldrich 99%), urea [NH_2CONH_2] (Aldrich >99%), ZnO (Aldrich >99%) and CuO (Aldrich >99%) were used as received. In order to remove the water residue and trapped air, ChCl and urea were dried under vacuum at 333–363 K for at least 2 h. The eutectic solvent comprising 1:2 molar ratio of ChCl and urea (12CU) was stirred under argon atmosphere using a polytetrafluoroethylene (PTFE)-coated magnetic stir bar in a beaker at 353 K until a homogeneous, colorless ionic liquid formed. Then, powdered ZnO was added into the 12CU ionic liquid at different temperatures (313 to 353 K) and stirred until the ZnO-saturated electrolytes were achieved. The concentrations of the dissolved Zn species (mainly in the form of $[ZnClO\cdot urea]^-$) [32,33] in the ZnO-saturated 12CU ionic liquid at 313, 333 and 353 K were determined to be approximately 0.006, 0.122 and 0.553 M, respectively. It is obvious that the solubility of ZnO in 12CU increases with increasing temperature.

2.2. Electrochemical testing and electrodeposition

All electrochemical experiments including CV, chronoamperometry and potentiodynamic polarization were performed by using a BioLogic HCP-803 electrochemical workstation. A cylindrical glass breaker (100 mL) was used as the electrolytic cell. Approximately 50 mL of the preformed ZnO-saturated 12CU ionic liquid was used as electrolyte for the electrochemical experiments. The electrochemical processes were carried out under an argon gas atmosphere

during experiment. A three-electrode system was used for the electrochemical measurements and electrodeposition experiments. A platinum wire (1.6 mm in diameter) was used as counter electrode, a Cu electrode (0.5 mm in diameter) was employed as working electrode and a silver wire (0.5 mm in diameter) was served as reference electrode. All the electrodes were firstly mechanically polished and then immersed in 5% HCl for 1 min. Finally, the electrodes were rinsed with distilled water and dried before all measurements. The schematic illustration of the route for facile electrodeposition of Zn and Cu–Zn alloy films from ZnO and CuO precursors is shown in Fig. 1. The formed $[MClO{\cdot}urea]^{-}$ can react with Ch^{+} ions to form metals/alloys and $[ChCl{\cdot}O{\cdot}urea]^{2-}$ at cathode. Then, the generated complex $[ChCl{\cdot}O{\cdot}urea]^{2-}$ anion can diffuse through electrolyte to anode and lose electrons to produce gas [26]. The anode gas is mainly composed of O_2, and small amounts of Cl_2 may occur at anode if the applied potential is higher than the decomposition potential of the ionic liquid [35,36]. After electrodeposition experiments, the samples were cleaned with distilled water and acetone to completely remove the rest ionic liquid and subsequently dried under vacuum.

Potentiodynamic polarization experiments were carried out in a 3 wt% NaCl aqueous solution, a platinum wire was used as counter electrode and a saturated calomel electrode (SCE) was served as reference electrode. The electrodeposited Zn film with an exposed area of approximately 0.2 cm^2 was used as working electrode. Before the potentiodynamic sweep experiments, the working electrode was immersed into 3 wt% NaCl aqueous solution for about 20 min to stabilize the open-circuit potential (OCP). The OCPs of the Zn films electrodeposited under different cathodic potentials and temperatures tend to stabilize in the potential range from –0.69 to –1.05 V, and the OCP of the Cu substrate is stabilized at around –0.21 V after 20 min

of immersion. For the polarization test, the potential was swept from –0.3 V below OCP to +0.2 above OCP at a scan rate of 5 mV s^{-1}. The corrosion potential (E_{corr}) and corrosion current density (j_{corr}) were analyzed by Tafel extrapolation method.

2.3. Film characterization

The concentrations of the dissolved zinc species in the ZnO-saturated 12CU ionic liquid were analyzed by inductively coupled plasma spectroscopy (ICP, Perkin Elmer PE400). The surface morphology and elemental composition of the electrodeposited Zn and Cu–Zn alloy films were characterized using a JEOL JSM-6700F scanning electron microscope (SEM) accompanied with an energy dispersive X-ray spectrometer (EDS, Oxford INCA EDS system). The microstructure of the electrodeposited Zn films was further investigated using a transmission electron microscopy (TEM, JEOL JSM-2010F). The phase composition of the Zn films was determined by X-ray diffraction (XRD) using a Rigaku D/Max-2550 diffractometer with Cu Kα radiation.

3. Results and discussion

3.1. CV analysis

In order to investigate the electrochemical behavior of Zn, CV experiments using a Cu electrode as working electrode at different scan rates in 12CU–ZnO (0.1 M) were performed systematically, and the CV curves are shown in Fig. 2a. In 12CU–ZnO (0.1 M) system (see Fig. S1b in the supplementary material) at 333 K, the single cathodic current peak observed at about –1.12 V is attributed to the reduction of Zn^{2+} to the metal Zn, the anodic current peak occurred at approximately –0.65 V is due to the stripping of the electrodeposited Zn. The cathodic limit of pure 12CU is about –1.2 V (see Fig. S1a). The cathodic and anodic peak current densities increase with

the increase of scan rate, and the cathodic and anodic peak potentials shift to more negative and positive sides, respectively. A good linear relationship was obtained between the cathodic current density (j_p) and the square root of scan rate ($v^{1/2}$), as shown in Fig. 2b, indicating that the electrode reaction is mainly diffusion-controlled. The separation between the cathodic peak and half-peak potentials $|E_p - E_{p/2}|$ increases with the increase of scan rate. At the lowest scan rate, the separation of 56 mV is still larger than the value for the reversible process (31 mV at 333 K). All of these results indicat that the reduction reaction of Zn(II) to Zn in 12CU may be a diffusion-controlled quasi-reversible and it involves a one-step two electrons transfer process[37].

For a quasi-reversible charge transfer process, the diffusion coefficient of Zn(II) can be determined by the irreversible Randles-Sevick equation (1) [37], which is also applicable to the quasi-reversible systems [38,39],

$$i_p = 0.4958nFAC_{Zn(II)}D_{Zn(II)}^{1/2}\left(\frac{\alpha n_\alpha F v}{RT}\right)^{1/2} \quad (1)$$

where i_p is the cathodic peak current, n is the number of exchanged electrons, F is the Faraday constant, A is the electrode area, $C_{Zn(II)}$ is the Zn(II) species concentration, $D_{Zn(II)}$ is the diffusion coefficient of Zn(II) species, α is the tranfer coefficient, n_α is the electron transfer number in the rate determining step, v is the scan rate, R is the gas constant, T is the absolute temperature. The value α can be obtained from equation (2) [37]:

$$|E_p - E_{p/2}| = 1.857RT/\alpha n_\alpha F \quad (2)$$

where E_p and $E_{p/2}$ are the cathodic peak potential and half-peak potential, respectively. According to equation (2) and data obtained from Fig. 2a, the average tranfer coefficient can be calculated as 0.34. Substituting this and other parameters in equation (1), the diffusion coefficient of Zn(II) in 12CU is determined to be 1.65×10^{-8} cm^2 s^{-1} at 333 K, which is smaller than that of Zn(II) in $AlCl_3$-EMIC (2.6

× 10^{-6} cm^2 s^{-1} [40]) and Bu_3MeN-TFSI (1.6 × 10^{-7} cm^2 s^{-1} [41]) ionic liquids. The relatively low mobility of Zn(II) species may be attributed to the high viscosity of the 12CU [42] and the formation of large, sterically hindered Zn-complex anions when ZnO is dissolved in the 12CU [29].

3.2. Chronoamperometric investigations and nucleation-growth mechanism of Zn electrodeposition

In order to investigate the mechanism of the Zn nucleation-growth process in more detail, chronoamperometric experiments were conducted by negatively stepping the cathodic potentials that are sufficient to initiate nucleation-growth process. Typical current density–time transients recorded from the potential step experiments in 12CU–ZnO (0.1 M) at 333 K are shown in Fig. 3a. The initial regime of each transient is characterized by a sharp decrease in current density which may be caused by the double layer charging [43]. Then the current density increases which is attributed to the formation and growth of Zn nuclei, until a current density maximum, j_m, is reached at time, t_m. The j_m increases while the t_m shortens with an increase in the applied potential. The electrodeposition of metals onto foreign substrates generally involves some types of three-dimensional nucleation process accompanied diffusion-controlled hemispherical growth. Scharifker and Hills proposed two limiting models [44], including the instantaneous nucleation and progressive nucleation, to identify the nucleation mechanism. For instantaneous nucleation, all the Zn nuclei are created simultaneously at the beginning of the potential step, whereas in the progressive nucleation, new crystals are gradually created throughout chronoamperometric experiment. In order to differentiate the two nucleation-growth models, the data taken from the chronoamperometric experiments are compared with those obtained using theoretical transients. The theoretical

transients for limiting cases of instantaneous and progressive nucleation can be calculated using equation (3) and (4), respectively.

$$\left(j_{\text{inst}}/j_{\text{m}}\right)^2 = 1.9542\left(t/t_{\text{m}}\right)^{-1}\left\{1-\exp\left[-1.2564\left(t/t_{\text{m}}\right)\right]\right\}^2 \quad (3)$$

$$\left(j_{\text{prog}}/j_{\text{m}}\right)^2 = 1.2254\left(t/t_{\text{m}}\right)^{-1}\left\{1-\exp\left[-2.3367\left(t/t_{\text{m}}\right)^2\right]\right\}^2 \quad (4)$$

The comparison of the experimental current density–time transients with the theoretical models obtained from equation (3) and (4) are shown in Fig. 3b. It is obvious that the electrodeposition of Zn corresponds to the three-dimensional instantaneous nucleation-growth process. Besides, The value of $j_{\text{m}}^2 t_{\text{m}}$ are found to be independent of the cathodic electrodeposition potential, and the diffusion coefficient of Zn(II) for the instantaneous nucleation process can be calculated by using equation (5) [44,45].

$$j_{\text{m}}^2 t_{\text{m}} = 0.1629(nFc)^2 D \quad (5)$$

The average value of diffusion coefficient is 2.02×10^{-8} cm^2 s^{-1}, which is in good agreement with the result obtained from CV.

3.3. Electrodeposition of Zn films and morphology observation

Bulk electrodeposition of Zn films on Cu substrate can form adherent layers which possess striking brightness and silvery appearance. The surface morphologies of the Zn electrodeposits obtained at different cathodic potentials are shown in Fig. 4. It is obvious that the Zn electrodeposits obtained at –1.05 V appear to have uniform, dense and compact structure (Fig. 4a). When the electrodeposition potential extends to more negative at –1.10 V, the homogeneous hexagonal-shape particles begin to form (Fig. 4b). The electrodeposition potential on the working electrode acts as the main driving force for the electrodeposition of Zn particles, which plays an important role in changing the nucleation-growth of Zn particles. The current

density increases with increasing the electrodeposition potential, and the increase in current density is beneficial to the nucleation rate during the electrodeposition process. However, a further negative shift of the potential to –1.15 V results in nodular electrodeposits with different sizes (Fig. 4c). The sharp and elongated of Zn nanoparticles is due to the increase of the electrodeposition rate. It seems that more negative potential on the working electrode induces more nucleation sites on the substrate, which is beneficial for the nucleation process.

The surface morphologies of the Zn electrodeposits obtained at different electrodeposition temperatures are shown in Fig. 5. The electrodeposits obtained at the low temperature are flat and compact (Fig. 5a). When the temperature changes from 313 to 353 K, the particle size of the electrodeposited Zn seems to apparently increase. The viscosity of 12CU ionic liquid decreases with the increase of the electrodeposition temperature, therefore, the current densities increase with the increase of the temperature. As a result, the reaction rate and the growth of nuclei during the electrodeposition process increase with increasing the temperature, which leads to the electrodeposited Zn particles grow up to form larger particles. At 353 K (Fig. 5c), the particles of the electrodeposits show non-uniform structure compared to the other electrodeposits obtained at lower temperatures. These results indicate that higher temperature can enhance the reaction rate and further accelerate the growth of nuclei, which contribute to the formation of large particles. The average current efficiency and energy consumption of this process are calculated to be approximately 89.7% and 3.14 kWh/kg, respectively [46].

3.4. XRD and Cross-sectional TEM analysis

The XRD pattern of the Zn electrodeposits on Cu substrate obtained from 0.1 M ZnO in 12CU at –1.10 V and 333 K for 40 min are shown in Fig. 6. The XRD analysis indicates that all

the peaks are associated with Zn and Cu (substrate), no other peaks are observed. It is evidenced that the electrodeposited film is composed of high purity Zn, which can be further confirmed by the EDS analysis (see Fig. S2).

Fig. 7a is the SEM characterizations of the hexagonal-shape Zn films electrodeposited at –1.10 V and 333 K for 40 min, it can be observed that the particle size of the electrodeposits is approximately 200 nm. The average crystal size of the Zn phase was calculated using Scherrer equation [47] with TOPAS software based on the XRD data (Fig. 6), and the calculated value is approximately 25.7 nm, which indicating that the hexagonal-shape Zn particles are formed due to the agglomeration of Zn crystals [48]. Moreover, the texture coefficient was also calculated and the value of 2.01 matches the preferred growth in the (101) direction [49]. Fig. 7b–7d shows the cross-sectional TEM images of the electrodeposited Zn film on Cu substrate. As shown in Fig. 7b, the interface of the Zn film and Cu substrate can be clearly distinguished as labelled by a dashed line. The Cu substrate has a coarse particle structure, and no obvious gaps or pores are observed in the Zn film. Moreover, the average thickness of the electrodeposited Zn film is approximately 40 nm. It should be noted that the deposited Pt thin film was served as a protection layer for the Zn film when preparing the cross-sectional TEM sample. Fig. 7c shows the high revolution (HR)-TEM image of the Zn film/Cu substrate interface. The left part of Fig. 7c is confirmed to be Zn film by EDS and the right part is Cu substrate. The HR-TEM image of the Zn crystals exhibits ordered structure, from which it can be seen that the expanded plane fringe with 0.211 nm crystal plane spacing can be assigned to the Zn (101) plane. In addition, the indexed spot of the selected area electron diffraction (SAED) patterns in Fig. 7d also indicates the nanocrystal structure of the Zn film and the coarse grain structure of Cu

substrate [50]. The SAED patterns also confirm the hcp structure of the Zn electrodeposit on the Cu substrate.

3.5. Corrosion behavior of the electrodeposited Zn films

Fig. 8 reveals the typical potentiodynamic polarization curves of the Zn films electrodeposited under different conditions and the blank Cu substrate in 3 wt% NaCl aqueous solution at room temperature. The cathodic reaction in the polarization curves corresponds to the hydrogen evolution, and the anodic branch corresponds to the corrosion resistance. Corrosion potentials (E_{corr}) and corrosion current densities (j_{corr}) derived from the polarization curves through Tafel extrapolation are summarized in Table 1. For the blank Cu substrate, a remarkable anodic reaction occurs when the applied potential moves to the anodic area, the polarization current increases with more positive anodic potential. The corrosion rate is proportional to the corrosion current density. Among the five electrodeposited Zn films, the Zn film electrodeposited at 353 K and –1.10 V exhibits the highest j_{corr} of about 50.19 μA cm^{-2}, which is close to the Cu substrate. The poor corrosion resistance of the Zn film electrodeposited at 353 K and –1.10 V may be due to its coarse particle structure of Zn (Fig. 5c). The Zn films electrodeposited at more positive potentials and low temperatures have lower values of j_{corr} (Table 1). The j_{corr} value of the Zn film electrodeposited at 333 K and –1.05 V is decreased to about 12.05 μA cm^{-2}. The improved corrosion resistance may be attributed to the dense and compact structure of the Zn film (Fig. 4a) [51].

3.6. Electrodeposition of Cu–Zn alloy films

3.6.1. Voltammetric study

Typical CV curve of the 12CU ionic liquid dissolved with 0.1 M ZnO and 0.01 M CuO on a Cu

electrode at 333 K is shown in Fig. 9. There are three reduction peaks on the cathodic branch of the voltammogram. One small reduction peak at –0.15 V (labeled as c_1) is attributed to the Cu(II) to Cu(I) reduction process, and the reduction peak at –0.50 V (c_2) is assigned to the Cu(I) to Cu reduction process. The evident reduction peak at –1.15 V (c_3) can be attributed to the Zn(II) to Zn reduction process. When the scan reversed, four oxidation peaks (a_1, a_2, a_3 and a_4) are observed in the potential range of –1.00 to 0.60 V. The oxidation peaks (a_1 and a_2, a_4) at approximately 0.45, –0.2 and –0.75 V correspond to the stripping potential of pure Cu (a_1 and a_2) and Zn (a_4), respectively, and the oxidation peak (a_3) between a_4 and a_2 is mainly attributed to the stripping of Cu–Zn electrodeposits.

3.6.2. Characterization of the Cu–Zn electrodeposits

Fig. 10a shows the XRD patterns of the Cu–Zn alloy electrodeposited on a Cu substrate in the 12CU ionic liquid containing 0.1 M ZnO and 0.01 M CuO at different cathodic potentials and 333 K for 100 min. The XRD analysis shows that the dominate phases of the Cu–Zn film electrodeposited at –1.10 V are Cu_5Zn_8 and Cu (substrate), which further confirms that Cu–Zn codeposition can be achieved through the effectively control of electrodeposition potential. When the electrodeposition potential changes from –1.10 to –1.15 V, it is noticeable that the XRD pattern of the film obtained at –1.15 V is much different from that of the film electrodeposited at –1.10 V. Two new phases ($CuZn_5$, Zn) are observed and the Cu_5Zn_8 phase is disappeared, which is mainly due to the Zn electrodeposition rate obviously increases with more negative potential. The obtained phases of the Cu–Zn films electrodeposited on a Fe substrate under the above conditions are the same as the electrodeposits on the Cu substrate (see Fig. S3), which indicates that the phase compositions of the Cu–Zn alloy cannot be affected by the metal substrates. The average crystal sizes of the Cu_5Zn_8, $CuZn_5$ and Zn phases calculated

according to Scherrer equation [47] with TOPAS software based on the XRD data (Fig. 10a) are 40.0, 51.5 and 64.0 nm, respectively, which indicate that the Cu–Zn alloy particles are formed due to the agglomeration of Cu and Zn crystals [48]. The surface morphologies of Cu–Zn alloys electrodeposited in the 12CU ionic liquid containing 0.1 M ZnO and 0.01 M CuO at different cathodic potentials and 333 K for 100 min were further characterized and shown in Fig. 10b and 10c. The Cu–Zn deposit obtained at –1.10 V is composed of spherical clusters with some void space between the particles (Fig. 10b). With increasing the potential to –1.15 V, some polygonal structure of particles begin to form, and the electrodeposits are flat and compact (Fig. 10c).

4. Conclusions

The electrodeposition of Zn and Cu–Zn alloy from ZnO/CuO precursors has been investigated in ChCl/urea-based DES. Electrochemical measurements showed that the Zn electrodeposition is a diffusion-controlled quasi-reversible, one-step, two electrons transfer process. The diffusion coefficient of Zn(II) was estimated to be 1.65×10^{-8} cm^2 s^{-1} at 333 K. Three-dimensional instantaneous nucleation with diffusion-controlled growth process occurred during Zn electrodeposition and the diffusion coefficient of Zn(II) showed good agreement with the result of CV. Uniform, dense and compact Zn electrodeposits can form under more positive potentials and lower temperatures. Non-uniform and clustering Zn electrodeposits with different particle sizes can form under more negative potentials and higher temperatures. The average current efficiency and energy consumption of this process are calculated to be approximately 89.7% and 3.14 kWh/kg, respectively. Meanwhile, the electrodeposited Zn crystals preferentially orient parallel to the (101) plane. Furthermore, the Zn films obtained under more positive potentials and low temperatures exhibit improved corrosion resistance in 3 wt% NaCl

aqueous solution, which is mainly attributed to the flat, compact and fine particles in the film. In addition, the Cu–Zn alloy films have also been electrodeposited directly from their metal oxide precursors in 12CU electrolyte and the phase composition of the Cu-Zn alloy depends on the electrodeposition potential, which may have implications for the electrodeposition of other alloys films from oxides precursors in DESs system.

Acknowledgments

The authors thank China National Funds for Distinguished Young Scientists (No. 51225401), the National Natural Science Foundation of China (Nos. 51304132 and 51574164), the National Basic Research Program of China (No. 2014CB643403), the Science and Technology Commissions of Shanghai Municipality (No. 14JC1491400), and the Young Teacher Training Program of Shanghai Municipal Education Commission for financial support. We also thank the Instrumental Analysis and Research Center of Shanghai University for materials characterization.

References

[1] H.Q. Liu, S. Szunerits, W.G. Xu, R. Boukherroub, Preparation of superhydrophobic coatings on zinc as effective corrosion barriers, ACS Appl. Mat. Interfaces 1 (2009) 1150–1153.

[2] Z. Liu, S.Z.E. Abedin, F. Endres, Electrodeposition and stripping of zinc from an ionic liquid polymer gel electrolyte for rechargeable zinc-based batteries, J. Solid State Electrochem. 18 (2014) 2683–2691.

[3] S. Fashu, C.D. Gu, X.L. Wang, J.P. Tu, Influence of electrodeposition conditions on the microstructure and corrosion resistance of Zn–Ni alloy coatings from a deep eutectic solvent, Surf. Coat. Technol. 242 (2014) 34–41.

[4] A.P. Brown, J.H. Melsenhelder, N.P. Yao, The alkaline electrolytic process for zinc production: a critical evaluation, Ind. Eng. Chem. Prod. Res. Dev. 22 (1983) 263–272.

[5] P. Guillaume, N. Leclerc, C. Boulanger, J.M. Lecuire, F. Lapicque, Investigation of optimal conditions for zinc electrowinning from aqueous sulfuric acid electrolytes, J. Appl. Electrochem. 37 (2007) 1237–1243.

[6] H. Yan, J. Downes, P.J. Boden, S.J. Harris, A model for nanolaminated growth patterns in Zn and Zn–Co electrodeposits, J. Electrochem. Soc. 143 (1996) 1577–1583.

[7] A. Gomes, M.I. da Silva Pereira, Pulsed electrodeposition of Zn in the presence of surfactants, Electrochim. Acta 51 (2006) 1342–1350.

[8] D.J. Mackinnon, J.M. Brannen, R.C. Kerby, The effect of lead on zinc deposit structures obtained from high purity synthetic and industrial acid sulphate electrolytes, J. Appl. Electrochem. 9 (1979) 55–70.

[9] A.M. Abdelkader, K.T. Kilby, A. Cox, D.J. Fray, DC voltammetry of electro-deoxidation of solid oxides, Chem. Rev. 113 (2013) 2863–2886.

[10] X.L. Zou, X.G. Lu, Z.F. Zhou, W. Xiao, Q.D. Zhong, C.H. Li, W.Z. Ding, Electrochemical extraction of Ti_5Si_3 silicide from multicomponent Ti/Si-containing metal oxide compounds in molten salt, J. Mater. Chem. A 2 (2014) 7421–7430.

[11] X.L. Zou, S.L. Gu, H.W. Cheng, X.G. Lu, Z.F. Zhou, C.H. Li, W.Z. Ding, Facile electrodeposition of iron films from $NaFeO_2$ and Fe_2O_3 in alkaline solutions, J. Electrochem. Soc. 162 (2015) D49–D55.

[12] F. Endres, D.R. MacFarlane, A.P. Abbott (Eds.), Electrodeposition from Ionic Liquids, Wiley-VCH Verlag, Weinheim, 2008.

[13] E.W. Castner Jr., J.F. Wishart, Spotlight on ionic liquids, J. Chem. Phys. 132 (2010) 120901–120909.

[14] J.M. Hartley, C.-M. Ip, G.C.H. Forrest, K. Singh, S.J. Gurman, K.S. Ryder, A.P. Abbott, G. Frisch, EXAFS Study into the speciation of metal salts dissolved in ionic liquids and deep eutectic solvents, Inorg. Chem. 53 (2014) 6280–6288.

[15] J. Dogel, W. Freyland, Layer-by-layer growth of zinc during electrodeposition on Au(111) from a room temperature molten salt, Phys. Chem. Chem. Phys. 5 (2003) 2484–2487.

[16] S.-I. Hsiu, J.-F. Huang, I.-W. Sun, C.-H. Yuan, J. Shiea, Lewis acidity dependency of the electrochemical window of zinc chloride–1-ethyl-3-methylimadazolium chloride ionic liquids, Electrochim. Acta 47 (2002) 4367–4372.

[17] A.P. Abbott, J.C. Barron, K.S. Ryder, Electrolytic deposition of Zn coatings from ionic liquids based on choline chloride, Trans. Inst. Met. Finish. 87 (2009) 201–207.

[18] A.H. Whitehead, M. Pölzler, B. Gollas, Zinc Electrodeposition from a deep eutectic system containing choline chloride and ethylene glycol, J. Electrochem. Soc. 157 (2010) D328–D334.

[19] A.P. Abbott, J.C. Barron, G. Frisch, S. Gurman, K.S. Ryder, A.F. Silva, Double layer effects on metal nucleation in deep eutectic solvents, Phys. Chem. Chem. Phys. 13 (2011) 10224–10231.

[20] A.P. Abbott, J.C. Barron, G. Frisch, K.S. Ryder, A.F. Silva, The effect of additives on zinc electrodeposition from deep eutectic solvents, Electrochim. Acta 56 (2011) 5272–5279.

[21] N.M. Pereira, P.M.V. Fernandes, C.M. Pereira, A.F. Silva, Electrodeposition of zinc from choline chloride-ethylene glycol deep eutectic solvent: effect of the tartrate ion, J. Electrochem. Soc. 159 (2012) D501–D506.

[22] T.J. Simons, A.A.J. Torriero, P.C. Howlett, D.R. MacFarlane, M. Forsyth, High current density, efficient cycling of Zn^{2+} in 1-ethyl-3-methylimidazolium dicyanamide ionic liquid: the effect of Zn^{2+} salt and water concentration, Electrochem. Commun. 18 (2012) 119–122.

[23] Z. Liu, S.Z.E. Abedin, F. Endres, Electrodeposition of zinc films from ionic liquids and ionic liquid/water mixtures, Electrochim. Acta 89 (2013) 635–643.

[24] Y. Zheng, K. Dong, Q. Wang, S.J. Zhang, Q.Q. Zhang, X.M. Lu, Electrodeposition of zinc coatings from the solutions of zinc oxide in imidazolium chloride/urea mixtures, Sci. China: Chem. 55 (2012) 1587–1597.

[25] H.X. Yang, R.G. Reddy, Electrochemical kinetics of reduction of zinc oxide to zinc using 2:1 urea/ChCl ionic liquid, Electrochim. Acta 178 (2015) 617–623.

[26] H.X. Yang, R.G. Reddy, Electrochemical deposition of zinc from zinc oxide in 2:1 urea/choline chloride ionic liquid, Electrochim. Acta 147 (2014) 513–519.

[27] J.J. Ru, Y.X. Hua, C.Y. Xu, J. Li, Y. Li, D. Wang, C.C. Qi, Y.F. Jie, Morphology-controlled preparation of lead powders by electrodeposition from different PbO-containing choline chloride-urea deep eutectic solvent, Appl. Surf. Sci. 335 (2015) 153–159.

[28] J.J. Ru, Y.X. Hua, C.Y. Xu, J. Li, Y. Li, D. Wang, Z.R. Zhou, K. Gong, Preparation of porous lead from shape-controlled PbO bulk by in situ electrochemical reduction in ChCl–EG deep eutectic solvent, Appl. Surf. Sci. 357 (2015) 2094–2102.

[29] T. Tsuda, L.E. Boyd, S. Kuwabata, C.L. Hussey, Electrochemistry of copper(I) oxide in the 66.7–33.3 mol % urea–choline chloride room-temperature eutectic melt, J. Electrochem. Soc. 157 (2010) F96–F103.

[30] Q.B. Zhang, R. Wang, K.H. Chen, Y.X. Hua, Electrolysis of solid copper oxide to copper in choline chloride-EG eutectic melt, Electrochim. Acta 121 (2014) 78–82.

[31] Q.B. Zhang, A.P. Abbott, C. Yang, Electrochemical fabrication of nanoporous copper films in choline chloride–urea deep eutectic solvent, Phys. Chem. Chem. Phys. 17 (2015) 14702–14709.

[32] A.P. Abbott, G. Capper, D.L. Davies, R.K. Rasheed, P. Shikotra, Selective extraction of metals from mixed oxide matrixes using choline-based ionic liquids, Inorg. Chem. 44 (2005) 6497–6499.

[33] A.P. Abbott, G. Capper, D.L. Davies, K.J. McKenzie, S.U. Obi, Solubility of metal oxides in deep eutectic solvents based on choline chloride, J. Chem. Eng. Data 51 (2006) 1280–1282.

[34] A.P. Abbott, J. Collins, I. Dalrymple, R.C. Harris, R. Mistry, F. Qiu, J. Scheirer, W.R. Wise, Processing of electric arc furnace dust using deep eutectic solvents, Aust. J. Chem. 62 (2009) 341–347.

[35] K. Haerens, E. Matthijs, K. Binnemans, B. Van der Bruggen, Electrochemical decomposition of choline chloride based ionic liquid analogues, Green Chem. 11 (2009) 1357–1365.

[36] H.J. Sun, L.P. Yu, X.B. Jin, X.H. Hu, D.H. Wang, G.Z. Chen, Unusual anodic behaviour of chloride ion in 1-butyl-3-methylimidazolium hexafluorophosphate, Electrochem. Commun. 7 (2005) 685–691.

[37] A.J. Bard, L.R. Faulkner, Electrochemical methods: Fundamentals and Applications, J. Wiley & Sons, New York, 2000.

[38] R. Nagaishi, M. Arisaka, T. Kimura, Y. Kitatsuji, Spectroscopic and electrochemical properties of europium (III) ion in hydrophobic ionic liquids under controlled condition of water content, J. Alloys Compd. 431 (2007) 221–225.

[39] S.A. Kuznetsov, M. Gaune-Escard, Kinetics of electrode processes and thermodynamic properties of europium chlorides dissolved in alkali chloride melts, J. Electroanal. Chem. 595 (2006) 11–22.

[40] W.R. Pitner, C.L. Hussey, Electrodeposition of zinc from the Lewis acidic aluminum chloride-1-methyl-3-ethylimidazolium chloride room temperature molten salt, J. Electrochem. Soc. 144 (1997) 3095–3103.

[41] P.Y. Chen, C.L. Hussey, The electrodeposition of Mn and Zn–Mn alloys from the room-temperature tri-1-butylmethylammonium bis((trifluoromethane)sulfonyl)imide ionic liquid, Electrochim. Acta 52 (2007) 1857–1864.

[42] A.P. Abbott, M. Azam, G. Frisch, J. Hartley, K.S. Ryder, S. Saleem, Ligand exchange in ionic systems and its effect on silver nucleation and growth, Phys. Chem. Chem. Phys. 15 (2013) 17314–17323.

[43] R.Q. Li, Q.W. Chu, J. Liang, Electrodeposition and characterization of Ni–SiC composite coatings from deep eutectic solvent, RSC Adv. 5 (2015) 44933–44942.

[44] B.R. Scharifker, G. Hills, Theoretical and experimental studies of multiple nucleation, Electrochim. Acta 28 (1983) 879–889.

[45] G. Gunawardena, G. Hills, I. Montenegro, B. Scharifker, Electrochemical nucleation: part I. general considerations, J. Electroanal. Chem. 138 (1982) 225–239.

[46] S. Gürmen, M. Emre, A laboratory-scale investigation of alkaline zinc electrowinning, Miner. Eng. 16 (2003) 559–562.

[47] P. Scherrer, Estimation of the size and internal structure of colloidal particles by means of röntgen, Nachr. Ges. Wiss. Göttingen 2 (1918) 96–100.

[48] A.A. Chaaya, R. Viter, M. Bechelany, Z. Alute, D. Erts, A. Zalesskaya, K. Kovalevskis, V. Rouessac, V. Smyntyna, P. Miele, Evolution of microstructure and related optical properties of ZnO grown by atomic layer deposition, Beilstein J. Nanotechnol. 4 (2013) 690–698.

[49] J.A.R. Márquez, C.M.B. Rodríguez, C.M. Herrera, E.R. Rosas, O.Z. Angel, O.T. Pozos, Effect of surface morphology of ZnO electrodeposited on photocatalytic oxidation of methylene blue dye part I: analytical study, Int. J. Electrochem. Sci. 6 (2011) 4059–4069.

[50] C. Fournier, F. Favier, Zn, Ti and Si nanowires by electrodeposition in ionic liquid, Electrochem. Commun. 13 (2011) 1252–1255.

[51] S.G. Wang, C.B. Shen, K. Long, H.Y. Yang, F.H. Wang, Z.D. Zhang, Preparation and

electrochemical corrosion behavior of bulk nanocrystalline ingot iron in HCl acid solution, J. Phys. Chem. B 109 (2005) 2499–2503.

Table Caption

Table 1 Corrosion characteristics of Zn films and Cu substrate summarized from potentiodynamic polarization tests in 3 wt% NaCl solution.

Conditions	E_{corr}/mV	j_{corr}/μA cm^{-2}
333 K, –1.05 V	–806	12.05
333 K, –1.10 V	–977	28.92
333 K, –1.15 V	–1127	46.80
313 K, –1.10 V	–688	14.43
353 K, –1.10 V	–1085	50.19
Cu substrate	–216	63.54

Figure Captions

Fig. 1. Schematic illustration of the electrodeposition of Zn and Cu–Zn alloy films from metal oxides (MOs, *i.e.*, ZnO and CuO) precursors in 12CU ionic liquid.

Fig. 2. (a) CV curves of a Cu electrode in 12CU–ZnO (0.1 M) at 333 K with different scan rates. The scan rates were 5, 10, 15, 20 and 25 mV s^{-1}, respectively. (b) Relationship between cathodic peak current density (j_p) and square root of scan rate ($v^{1/2}$) calculated from (a).

Fig. 3. (a) Current density–time transients of chronoamperometric experiments on a Cu electrode in 12CU–ZnO (0.1 M) at different cathodic potentials from –1.05 to –1.15 V at 333 K. **(**b) Comparison of the dimensionless experimental curves derived from the current density–time transients shown in **(**a) with the theoretical models for instantaneous and progressive nucleations.

Fig. 4. SEM images of the Zn electrodeposits obtained from 12CU–ZnO (0.1 M) at 333 K on a Cu substrate at different cathodic potentials: (a) –1.05 V, (b) –1.10 V, (c) –1.15 V for 100 min.

Fig. 5. SEM images of the Zn electrodeposits obtained from 12CU–ZnO (0.1 M) at –1.10 V on a Cu substrate at different temperatures: (a) 313 K, (b) 333 K, (c) 353 K for 100 min.

Fig. 6. XRD pattern of the Zn electrodeposits obtained from 12CU–ZnO (0.1 M) on a Cu substrate at –1.10 V and 333 K for 40 min.

Fig. 7. (a) SEM image of the Zn electrodeposits obtained on a Cu substrate at –1.10 V and 333 K for 40 min. (b) TEM image of the cross-sectional of the electrodeposited Zn film on a Cu substrate corresponding to (a). (c) HR-TEM image of the electrodeposited Zn film/Cu substrate recorded from (b). (d) The selected area electron diffraction (SAED) pattern of the Zn electrodeposits corresponding to (c), and the (102), (101), (100) and (002) planes for Zn are

labelled in the figure.

Fig. 8. Typical potentiodynamic polarization curves of the Zn films electrodeposited under different conditions and the blank Cu substrate in 3 wt% NaCl aqueous solution at room temperature.

Fig. 9. CV curve of a Cu electrode in 12CU ionic liquid containing 0.1 M ZnO and 0.01 M CuO at 333 K with a scan rate of 10 mV s^{-1}.

Fig. 10. (a) XRD patterns of the Cu–Zn alloy electrodeposited on a Cu substrate in the 12CU ionic liquid containing 0.1 M ZnO and 0.01 M CuO at different cathodic potentials and 333 K for 100 min. (b) and (c) SEM images of the Cu–Zn electrodeposits obtained on a Cu substrate in the 12CU ionic liquid containing 0.1 M ZnO and 0.01 M CuO at 333 K for 100 min, (b) –1.10 V, (c) –1.15 V.

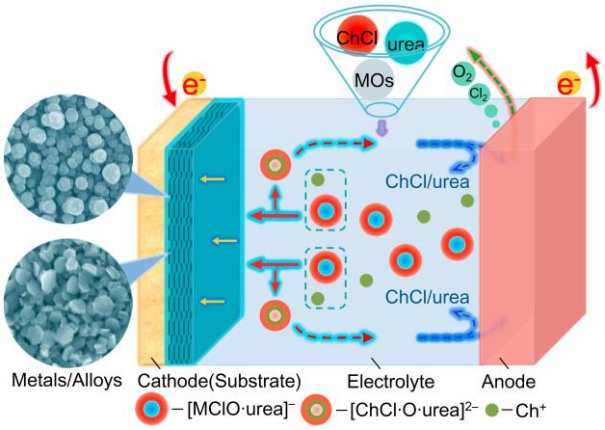

Fig. 1

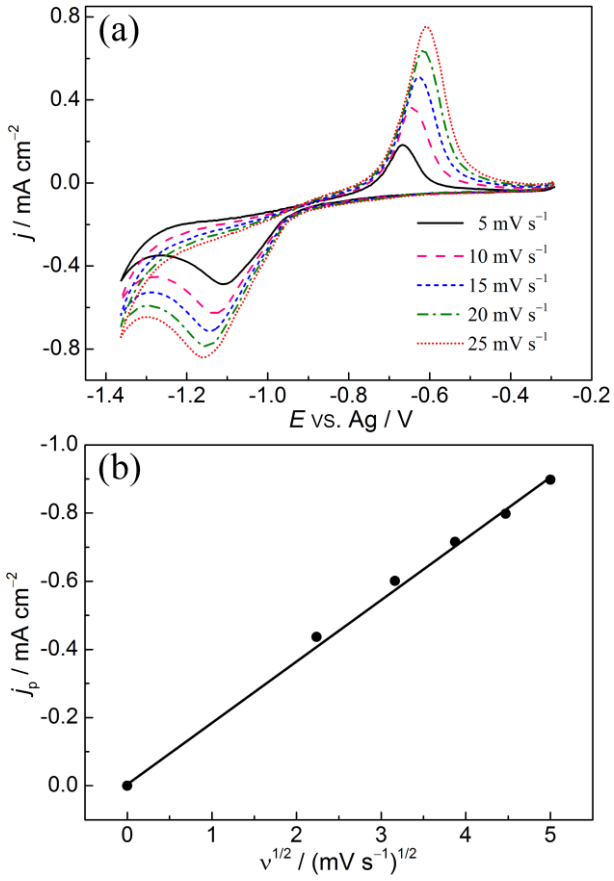

Fig. 2

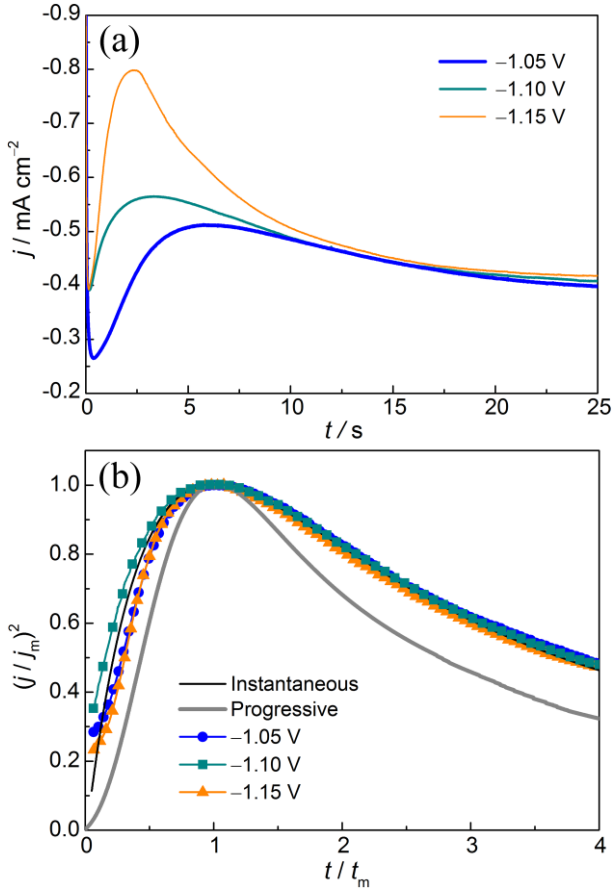

Fig. 3

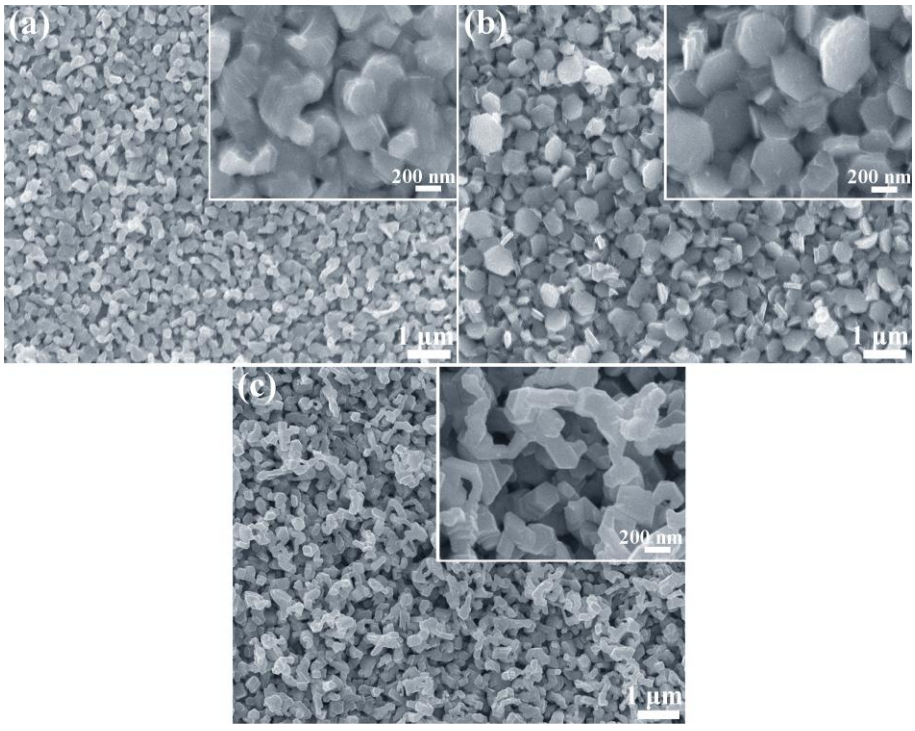

Fig. 4

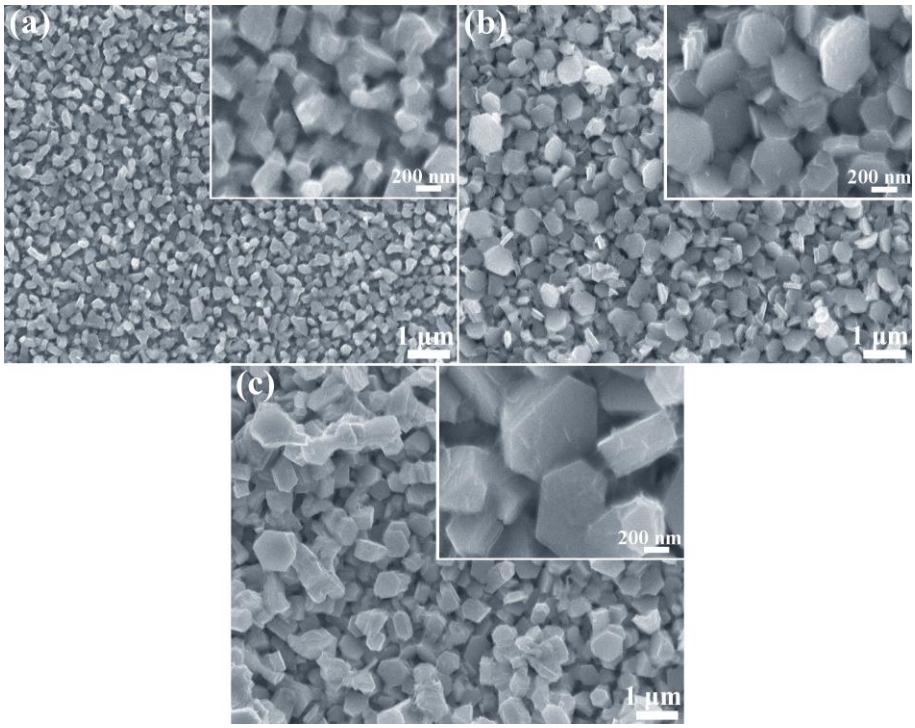

Fig. 5

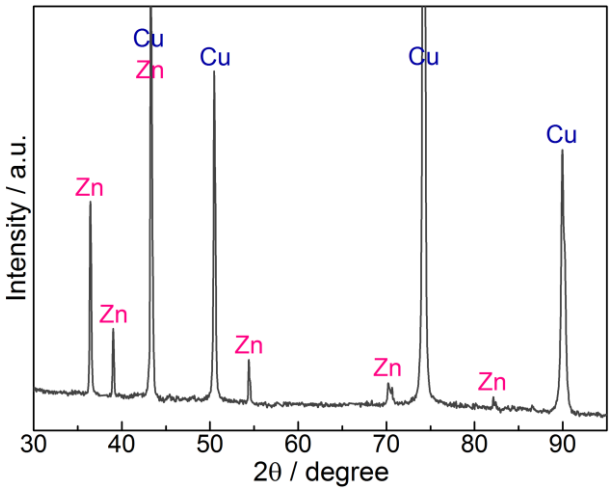

Fig. 6

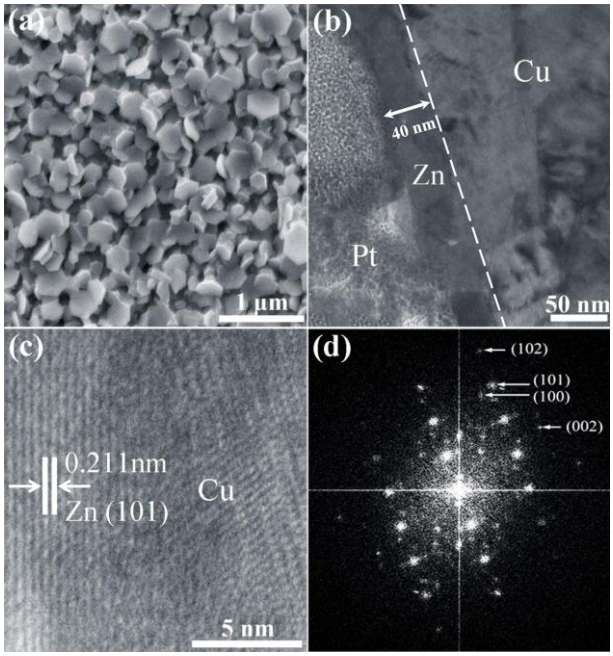

Fig. 7

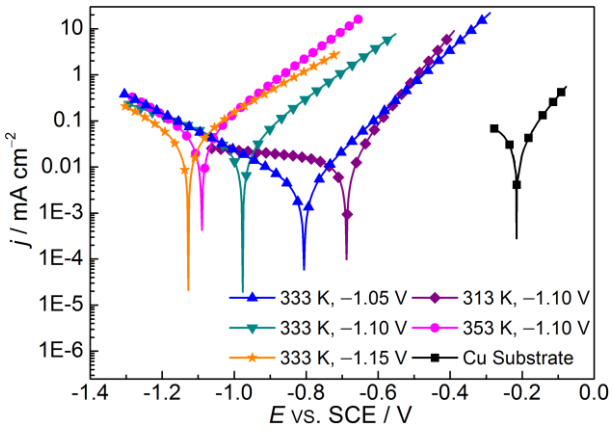

Fig. 8

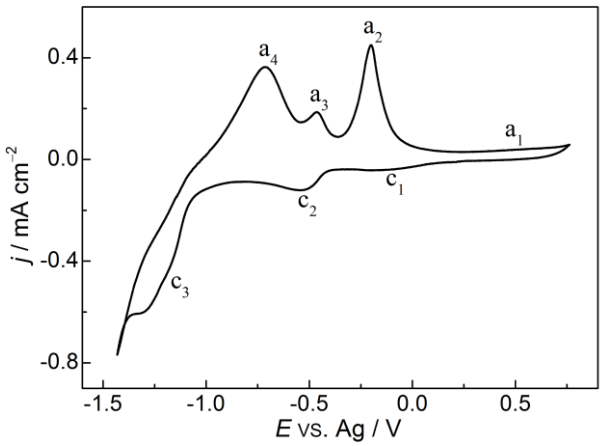

Fig. 9

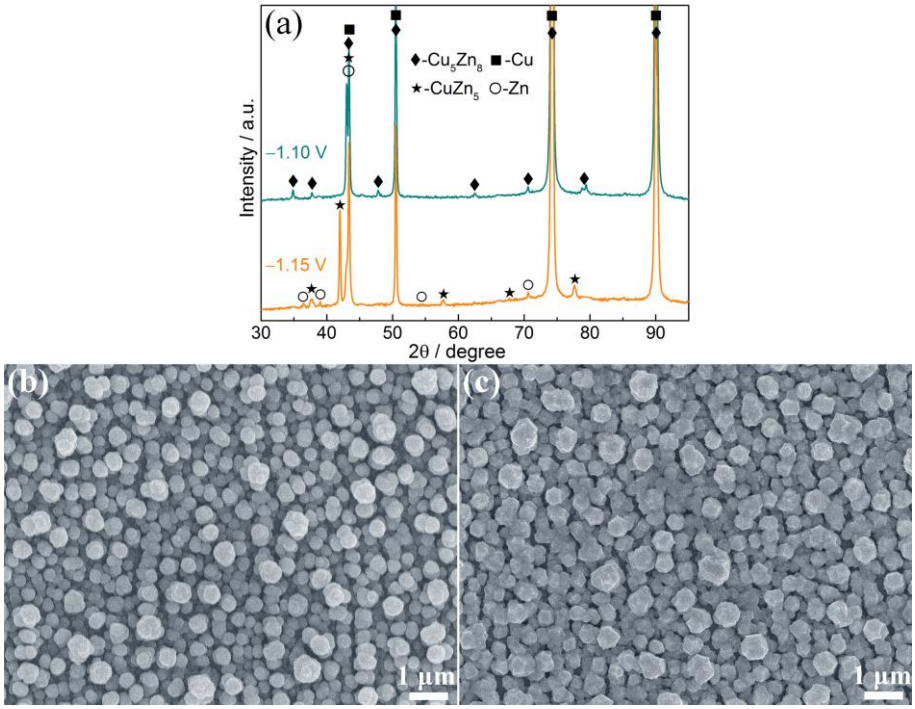

Fig. 10